# FTIR Study of the L Intermediate of *Anabaena* Sensory Rhodopsin: Structural Changes in the Cytoplasmic Region†

Akira Kawanabe,‡ Yuji Furutani,‡ Sa Ryong Yoon,|| Kwang-Hwan Jung,|| and Hideki Kandori*,‡

*Department of Frontier Materials, Nagoya Institute of Technology, Showa-ku, Nagoya, 466-8555, Japan, and Department of Life Science and Interdisciplinary Program of Integrated Biotechnology, Sogang University, Shinsu-Dong 1, Mapo-Gu, Seoul, 121-742, Korea*

*Received May 20, 2008; Revised Manuscript Received July 31, 2008*

ABSTRACT: *Anabaena* sensory rhodopsin (ASR) is an archaeal-type rhodopsin found in eubacteria. The gene encoding ASR forms a single operon with ASRT (ASR transducer) that is a 14 kDa soluble protein, suggesting that ASR functions as a photochromic sensor by activating the soluble transducer. One of the characteristics of ASR is that the formation of the M intermediate accompanies a proton transfer from the Schiff base to Asp217 in the cytoplasmic side [Shi, L., Yoon, S. R., Bezerra, A. G., Jr., Jung, K. H., and Brown, L. S. (2006) *J. Mol. Biol. 358*, 686−700], in remarkable contrast to other archaeal-type rhodopsins such as a light-driven proton-pump, bacteriorhodopsin (BR). In this study, we applied low-temperature Fourier transform infrared (FTIR) spectroscopy to the all-*trans* form of ASR at 170 K, and compared the structural changes in the L intermediate with those of BR. The $ASR_L$ minus ASR difference spectra were essentially similar to those for BR, suggesting common structures for the L state in ASR and BR. On the other hand, unique C═O stretching bands of a protonated carboxylic acid were observed at 1722 (+) and 1703 (−) $cm^{-1}$ at pH 5 and 7, and assigned to Glu36 by use of mutants. Glu36 is located at the cytoplasmic side, and the distance from the Schiff base is about 20 Å. This result shows the structural changes at the cytoplasmic surface in $ASR_L$. pH-dependent frequency change was also observed for a water stretching vibration, suggesting that the water molecule is involved in a hydrogen-bonding network with Glu36 and Asp217. Unique hydrogen-bonding network in the cytoplasmic domain of ASR will be discussed.

Four archaeal-type rhodopsins [bacteriorhodopsin (BR[1]), halorhodopsin (HR), sensory rhodopsin I (SRI), and sensory rhodopsin II (SRII) (also called phoborhodopsin)] were discovered in the cytoplasmic membrane of *Halobacterium salinarum* (*1*−*4*). The former two rhodopsins (BR and HR) function as light-driven proton and chloride pumps, respectively, while the latter two rhodopsins (SRI and SRII) act as photosensors responsible for attractant or repellent phototaxis, respectively. They have been extensively studied as model systems converting light energy into electrochemical potential or relaying environmental signal into cytoplasm. On the other hand, genome sequencing projects and environmental genomics have recently revealed that archaeal-like rhodopsins also exist in *Eukarya* and *Eubacteria*. In eukaryotes, archaeal-type rhodopsins were found in fungi (*5*), green algae (*6, 7*), dinoflagellates (*8*), and cryptomonads (*9*). Eubacterial rhodopsins were found in both γ- and α-proteobacteria (*10*−*12*) as well as in *Anabaena (Nostoc)* sp. PCC7120, a freshwater cyanobacterium (*13*), where it was named *Anabaena* sensory rhodopsin (ASR).

The gene encoding ASR, which is a membrane protein of 261 residues (26 kDa), and a small gene ASRT encoding a soluble protein of 125 residues (14 kDa) are under the same promoter in a single operon (*13*). The opsin gene was expressed heterologously in *Escherichia coli* and in the presence of all-*trans* retinal formed a pink pigment ($\lambda_{max}$ 549 nm in the dark-adapted form). The previous study reported that coexpression with ASRT accelerated the photocycle (*13, 14*), suggesting physical interaction with ASR. Isothermal calorimetry measurements also showed ASR interacting with a tetramer of ASRT (*15*).

Archaeal-type rhodopsins generally possess all-*trans* or 13-*cis* retinal as the chromophore in the dark, and ASR was suggested to function as a photochromic sensor existing in both isomeric forms (*14, 16*). However, functionally important states known so far were only derived from the all-*trans* form for archaeal-type rhodopsins, and all the photocycles of the all-*trans* forms have a common mechanism. For instance, in the light-driven proton pump of BR, the stable photoproduct at the end of the functional cycle of the all-

† This work was supported in part by grants from Japanese Ministry of Education, Culture, Sports, Science, and Technology to H.K. (19370067 and 20050015) and Y.F. (19045015), the 21C Frontier Microbial Genomics and Applications Center Program, Ministry of Education, Science & Technology, Korea to K.-H.J., and Research Fellowships from the Japan Society for the Promotion of Science for Young Scientists to A.K.

* To whom correspondence should be addressed. Phone and fax: 81-52-735-5207. E-mail: kandori@nitech.ac.jp.

‡ Nagoya Institute of Technology.

|| Sogang University.

[1] Abbreviations: BR, bacteriorhodopsin; ASR, *Anabaena* sensory rhodopsin; ASRT, ASR transducer; $ASR_L$, the L intermediate of the all-*trans* ASR; $ASR_K$, the K intermediate of the all-*trans* ASR; $BR_L$, the L intermediate of BR; DM, *n*-dodecyl-β-D-maltoside; PC, L-α-phosphatidylcholine; HOOP, hydrogen-out-of-plane; FTIR, Fourier-transform infrared.

10.1021/bi800941a CCC: $40.75 
Published on Web 08/30/2008

*trans* form is 100% all-*trans*, i.e., it is truly cyclic. Surprisingly, our recent low-temperature UV−visible spectroscopy of ASR revealed that the stable photoproduct of the all-*trans* form is 100% 13-*cis*, and that of the 13-*cis* form is 100% all-*trans* (*17*). The complete photocycling for the proton pump in BR and the complete photochromism for the chromatic sensor of ASR are highly advantageous for their functions, and the unique photoreactions must have been acquired for each rhodopsin during evolution. One interesting aspect is that the protein structures are similar between ASR and BR (*16*), suggesting that distinct functions are determined by small differences.

To understand the details of light-induced structural changes of ASR, we applied low temperature FTIR spectroscopy to all-*trans* ASR, and compared the difference spectra at 77 K with those of BR (*18*). The K intermediate minus all-*trans* form ASR difference spectra showed that the retinal isomerizes from all-*trans* to distorted 13-*cis* form similar to BR. On the other hand, a remarkable difference between all-*trans* forms of ASR and BR was revealed in water bands. Although ASR possesses a water molecule between the Schiff base and its counterion Asp75 similar to BR (*16*), the O−D stretching bands of water molecules were observed only in the >2500 $cm^{-1}$ region for the all-*trans* form of ASR (*18*). We interpreted that fact as a weak hydrogen bonding of the bridged water in ASR originating from its unique geometry. Since ASR does not pump protons and the direction of the proton movement is toward the cytoplasmic side as inferred from the sign of the photoelectric signal (*13, 19*), the results support the working hypothesis that the existence of strongly hydrogen-bonded water molecules is essential for proton pumping activity in archaeal-type rhodopsins (*20*).

The M intermediate with the deprotonated Schiff base is an important state in proton transport and signal transduction. It has been known that the Schiff base proton is transferred to the counterion (Asp85 in BR) if it is deprotonated. In this case, the proton transfer is toward extracellular side. On the other hand, the previous time-resolved FTIR study of ASR by Shi et al. reported the proton transfer to Asp217 in the cytoplasmic side (*21*), though Asp75 works as the counterion of the Schiff base in ASR. No proton transfer to Asp75 was also reported by Bergo et al. (*22*). This may be reasonable, because another aspartate (Asp212 in BR) is replaced by proline in ASR, and Asp212 plays an important role in the proton transfer in BR (*23, 24*). On the other hand, Sineshchekov et al. reported that the direction of proton transfer was dependent on the sample conditions, where the direction is toward cytoplasmic and extracellular side for C-terminal truncated and full-length ASR, respectively (*25*). According to these results, native full-length ASR in *E. coli* cells exhibits proton transfer direction the same as in BR. Thus, the molecular mechanism of ASR activation remains yet unclear.

In the present paper, we applied low-temperature FTIR spectroscopy at 170 K to the dark-adapted ASR that has predominantly all-*trans* retinal (97%) (*26*). The obtained $ASR_L$ minus ASR spectra were similar between the full-length and C-terminally truncated ASR, implying similar protein structural changes for the L state. The $ASR_L$ minus ASR spectra were essentially similar to those of BR, but a unique spectral feature was observed in the carboxylic C=O stretching region. The bands at 1722 (+) and 1703 (−) $cm^{-1}$ were observed at pH 5, which was reduced at pH 7 and disappeared at pH 9. The mutation study successfully assigned the bands to the C=O stretch of Glu36. Interestingly, Glu36 is located at the cytoplasmic side, and the distance from the retinal Schiff base is about 20 Å (Figure 1). We also observed pH-dependent frequency change of a water stretching vibration, which is located near Glu36. Unique hydrogen-bonding network in the cytoplasmic domain of ASR will be discussed.

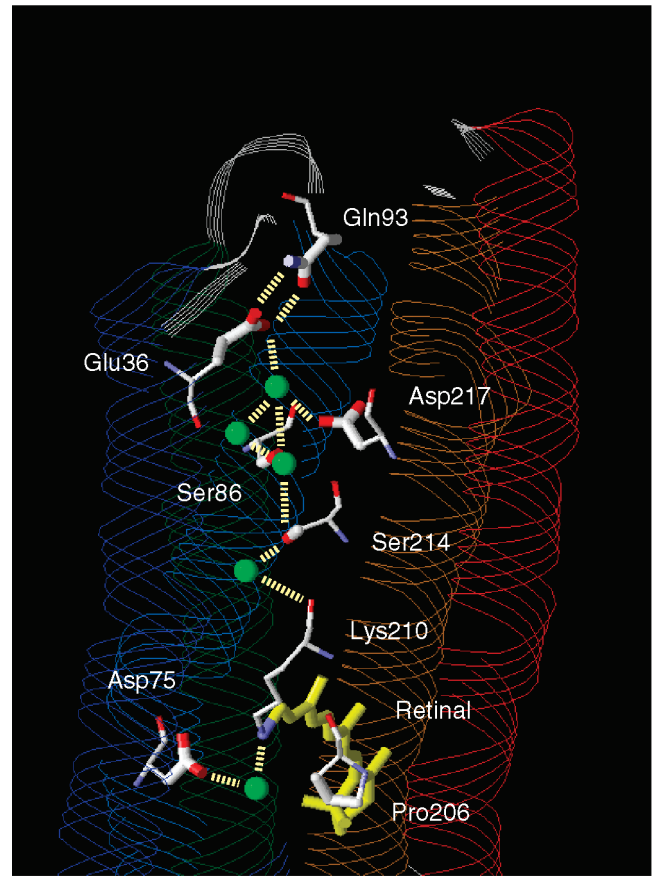


FIGURE 1: X-ray crystallographic structure of the cytoplasmic region of ASR (PDB entry 1XIO (*16*)). Top and bottom regions correspond to the cytoplasmic surface and retinal binding pocket, respectively. Green spheres represent water molecules in the cytoplasmic region. Hydrogen-bonds (yellow dashed lines) are inferred from the structure.

## MATERIALS AND METHODS

*Sample Preparation.* In the present study, we prepared C-terminally truncated and full-length ASR according to the method described previously (*13, 17, 27*). The E36Q and D217N mutants were designed based on the full-length ASR, which were produced by a two-step megaprimer PCR method (*28*), with two oligonucleotides (COSMO, Seoul, Korea): E36Q F-50-CAG TAC CAA TAC CTT GTG GCG ATG-30 and D217N R-50-GTA AAT TCA GAA AAA CTA AAT C-30. The final PCR products were cloned into plasmid pKJ606 (*29*), derived from pMS107, by replacing the original insert with *Xba*I/*Not*I digestion. After ligation the plasmids were transformed in *E. coli* strain DH5α. All of the mutations were confirmed by DNA sequencing (COSMO, Seoul, Korea). *E. coli* strain BL21 (Stratagene) was transformed

by introducing pMS107-derivative plasmid (*13*), which encodes the wild-type, E36Q and D217N opsin, and was grown in 2x YT medium in the presence of ampicillin (50 $\mu$g/ml) at 38 °C. Three hours after IPTG induction with addition of 10 $\mu$M all-*trans* retinal, pink-colored cells were harvested, sonicated, solubilized by 1% DM, and purified by a $Ni^{2+}$-NTA column. The purified ASR was then reconstituted into PC liposomes by removing the detergent with Bio-Beads, where the molar ratio of the added PC to ASR was 30:1. The liposomes were washed three times with a buffer [2 mM sodium phosphate (pH 7.0)]. A 40 $\mu$L aliquot was deposited on a $BaF_2$ window of 18 mm diameter and dried in a glass vessel that was evacuated by an aspirator.

*FTIR Spectroscopy.* FTIR spectroscopy was performed as described previously (*30*). The ASR film sample was hydrated with 1 $\mu$L of $H_2O$, $D_2O$, or $D_2{}^{18}O$ before the measurements. Then, the sample was placed in a cryostat (DN-1704, Oxford) mounted in the FTIR spectrometer (FTS-40, Bio-Rad). The cryostat was equipped with a temperature controller (ITC-4, Oxford), and the temperature was regulated with 0.1 K precision. All experimental procedures until setting the samples were performed in the dark or under dim red light (>670 nm).

Illumination with >580 nm light at 170 K for 16 min converted ASR to $ASR_L$. Each difference spectrum was calculated from two spectra constructed from 128 interferograms taken before and after the illumination. Three difference spectra obtained in this way were averaged to produce the $ASR_L$ minus ASR spectrum. The $BR_L$ minus BR spectra were taken from Kandori et al. (*30*).

## RESULTS

*Comparison of the Difference Infrared Spectra of the L Intermediate of Full-length ASR and Truncated ASR in the 1800−800 cm$^{-1}$ Region.* The previous photoelectric measurements showed that the direction of charge movement of full-length ASR was different from that of C-terminally truncated ASR (truncated ASR) for the L and M intermediates, whereas both charge movements were similar for the K intermediate (*25*). This suggests that full-length and truncated ASR have different structural changes in the L and M intermediates. Therefore, we prepared both full-length and truncated ASR, and measured the difference FTIR spectra for the L intermediate. Figure 2 compares the full-length $ASR_L$ minus ASR (solid line) and the truncated $ASR_L$ minus ASR (dotted line) spectra at 170 K upon hydration with $H_2O$. As is clearly seen, the spectrum of the full-length ASR is very similar to that of the C-terminally truncated ASR. Thus, the present FTIR spectra for the L intermediate showed no effects of the C-terminal truncation. All data below are shown for the full-length ASR including the mutant proteins. It should be noted that we confirmed similarity of the spectra at 170 K between full-length and truncated ASR at acidic and alkaline pH as well, though they could be different at room temperature.

*Comparison of the Difference Infrared Spectra of the L Intermediate of ASR and BR in the 1800−800 cm$^{-1}$ Region.* Figure 3 compares the $ASR_L$ minus ASR (a) and the $BR_L$ minus BR spectra (b) at 170 K. The samples were hydrated with $H_2O$ (solid lines) and $D_2O$ (dotted lines). In Figure 3a, the negative band at 1537 cm$^{-1}$ corresponds to the ethylenic

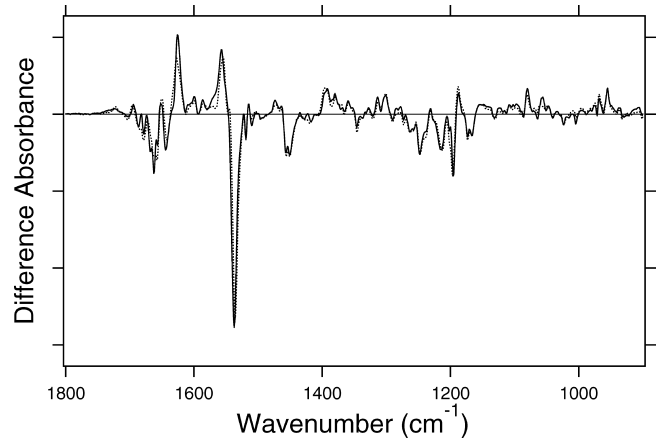


FIGURE 2: The full-length (solid line) and truncated (dotted line) $ASR_L$ minus ASR spectra (pH 7) in the 1800−900 cm$^{-1}$ region. The spectra are measured at 170 K upon hydration with $H_2O$. One division of the *y*-axis corresponds to 0.004 absorbance unit.

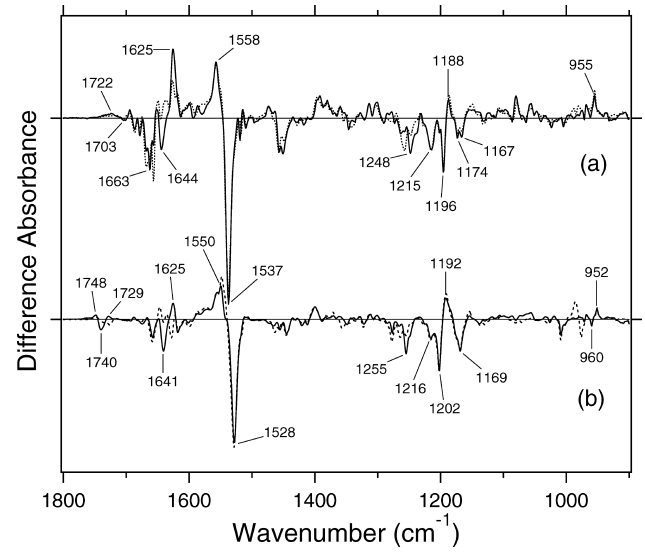


FIGURE 3: The $ASR_L$ minus ASR (a) and the $BR_L$ minus BR (b) spectra in the 1800−900 cm$^{-1}$ region, which are measured at pH 7 and 170 K upon hydration with $H_2O$ (solid line) and $D_2O$ (dotted line), respectively. One division of the *y*-axis corresponds to 0.012 absorbance unit.

vibration of all-*trans* retinal in ASR, which exhibits the absorption maximum at 549 nm (*26*). The $ASR_K$ minus ASR spectrum also showed the negative band at identical frequency (*18*). In the case of BR, the ethylenic vibration of the L intermediate is observed at higher frequency (1550 cm$^{-1}$) than that of the original state (1528 cm$^{-1}$), which corresponds to the blue-shifted absorption maximum of $BR_L$ (*31*). Similarly, illumination of ASR results in the spectral upshift to 1558 cm$^{-1}$. Blue-shifted visible absorption of $ASR_L$ is consistent with our low-temperature UV–visible analysis (*17*).

C−C stretching vibrations of retinal in the 1300−1150 cm$^{-1}$ region are sensitive to the local structure of the chromophore. Negative bands at 1255, 1216, 1202, and 1169 cm$^{-1}$ in Figure 3b were assigned to the C12−C13, C8−C9, C14−C15, and C10−C11 stretching vibrations of BR, respectively (*32*). These bands are typical to all-*trans* retinal protonated Schiff base but located at higher frequencies corresponding to charge delocalization in the retinal molecule in BR. $BR_L$ has a 13-*cis* retinal, resulting

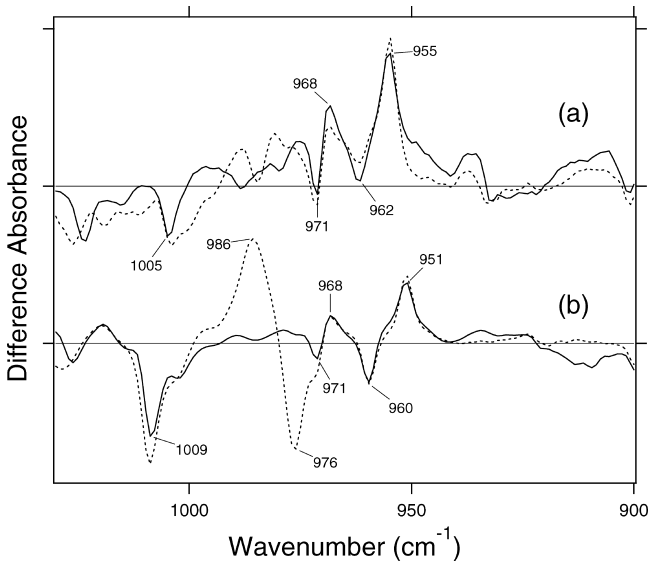


FIGURE 4: The $ASR_L$ minus ASR (a) and the $BR_L$ minus BR (b) spectra in the 1030−900 $cm^{-1}$ region, which correspond to hydrogen out-of-plane (HOOP) vibrations of the retinal chromophore. The sample was hydrated with $H_2O$ (solid lines) or $D_2O$ (dotted lines). One division of the *y*-axis corresponds to 0.0016 absorbance unit.

in the appearance of a strong positive band at 1192 $cm^{-1}$, which is assigned to C10−C11 and C14−C15 stretching vibrations (*33*). Essentially similar observation was obtained for ASR. From the similarity in frequency, negative bands at 1248, 1215, 1196, and 1174 (and/or 1167) $cm^{-1}$ can be assigned to C12−C13, C8−C9, C14−C15, and C10−C11 stretching vibrations of ASR (Figure 3a).

The difference spectra in the 1110−890 $cm^{-1}$ region are expanded in Figure 4, where hydrogen out-of-plane (HOOP), N−D in-plane bending and methyl rocking vibrations appear. The presence of strong HOOP modes represents the distortion of the retinal molecule (*34*). The $ASR_L$ minus ASR spectra exhibit two positive peaks at 968 and 955 $cm^{-1}$, which possibly correspond to the bands at 968 and 951 $cm^{-1}$ of $BR_L$, respectively (Figure 4). The bands at 986 (+) and 976 (−) $cm^{-1}$ were assigned to the N−D in-plane bending vibrations of $BR_L$ and BR, respectively (*35*). On the other hand, the $ASR_L$ minus ASR spectrum does not show clear H−D exchange-dependent bands in this region. The 1009 $cm^{-1}$ band in Figure 4b is insensitive to the H−D exchange and was assigned to the methyl rocking vibration of the retinal in BR. The band at 1005 $cm^{-1}$ in Figure 4a is also assignable to the methyl rocking vibration in ASR. Thus, similar L spectra were observed for ASR and BR.

Amide-I vibrations appear in the 1700−1550 $cm^{-1}$ region together with the C=N stretching vibration of the protonated retinal Schiff base (Figure 3). In general, the former is little sensitive to the H−D exchange, whereas the latter exhibits a downshift in $D_2O$. The bands at 1641 (−) and 1625 (+) $cm^{-1}$ were assigned to the C=N stretching vibrations of BR and $BR_L$, respectively (*33*). In the case of ASR, a prominent negative peak at 1644 $cm^{-1}$ is assignable to the C=N stretch of ASR, because the $D_2O$-sensitive 1644 $cm^{-1}$ band in the $ASR_K$ minus ASR spectra was identified by use of $^{15}N$-lysine labeled ASR (*26*). On the other hand, the C=N stretch of $ASR_L$ is not obvious. The positive peak at 1625 $cm^{-1}$ is a candidate, whereas the downshifted band was not clearly observed in $D_2O$ (dotted line in Figure 3a). The H−D independent band at 1663 $cm^{-1}$ presumably originates from amide-I vibration. The frequency suggests structural changes of a distorted α-helix. Since the negative band at 1663 $cm^{-1}$ is absent for the $ASR_K$ minus ASR spectra (*18*), the structural changes of α-helix newly appear in $ASR_L$.

*Comparison of the Difference Infrared Spectra of the L Intermediate in Protonated Carboxylic Acid (1800−1700 cm$^{-1}$) Region.* The infrared difference spectra in this frequency region mainly monitor the structural changes of protonated carboxylic acids. In the $BR_L$ minus BR difference spectra, the bands at 1748 (+) and 1729 (+) $cm^{-1}$ were assigned to the C=O stretching vibrations of the protonated Asp96 and Asp115, respectively, while large negative band at 1740 $cm^{-1}$ contains the corresponding bands of Asp96 and Asp115 in the unphotolyzed state (Figure 3b) (*36*). The corresponding amino acids in ASR are Ser86 and Asn105, so that we did not expect any peaks in this frequency region. Nevertheless, Figure 3a shows a broad positive peak at 1722 $cm^{-1}$ as well as a negative feature at 1703 $cm^{-1}$, suggesting structural perturbation of carboxylic acids upon formation of $ASR_L$. It should be noted that the bands do not originate from the contribution of $ASR_M$, because UV–visible spectroscopy confirmed no formation of $ASR_M$ at 170 K (*17*). The absence of a clear negative band at around 1400 $cm^{-1}$, characteristic of $COO^-$ stretching frequency of negatively charged carboxylates, suggests that appearance of the carboxylic C=O stretch at 1722 $cm^{-1}$ in $ASR_L$ is not due to the newly protonated species, but rather due to the frequency shift from 1703 $cm^{-1}$ in ASR (Figure 3a).

To further examine the spectral feature in this region, we measured $ASR_L$ minus ASR spectra at acidic (pH 5) and alkaline (pH 9) pH in addition to pH 7 (Figure 3a). We also measured the $ASR_L$ minus ASR spectra of D217N and E36Q mutant proteins to identify the responsible carboxylic acid. Figure 5 clearly shows that $ASR_L$ is formed at different pH values (5, 7, and 9 in a, b, and c, respectively), as well as for the D217N (d) and E36Q (e) mutants. Figure 6 highlights the carboxylic C=O stretching region, where all spectra were normalized by use of the negative 1196 $cm^{-1}$ band (Figure 5). Although the positive peak at 1722 $cm^{-1}$ was broad at pH 7 (Figure 6b), it was enhanced at pH 5 (Figure 6a). In contrast, the 1722 $cm^{-1}$ band completely disappeared at pH 9 (Figure 6c). Spectral downshift to 1717 $cm^{-1}$ in $D_2O$ (Figure 6a) is typical for carboxylic C=O stretching vibrations. Thus, we identify the positive band at 1722 $cm^{-1}$ in the $ASR_L$ minus ASR spectra as a carboxylic C=O stretch, whose $pK_a$ was estimated between 6 and 7.

The negative band at 1703 $cm^{-1}$ exhibits similar pH dependence to that of the 1722 $cm^{-1}$ band, being enhanced at pH 5, but disappearing at pH 9 (Figure 6a−c). In addition, the 1703 $cm^{-1}$ band is downshifted in $D_2O$ (Figure 6a), though the shifted negative band was not clearly observable because of the strong peaks at 1695 (+)/1687 (−) $cm^{-1}$ (Figure 3a). Similar pH dependence strongly suggests that the bands at 1722 (+)/1703 (−) $cm^{-1}$ originate from the same carboxylic group. The absence of pH dependent bands at around 1400 $cm^{-1}$ (Figure 5) also supports this interpretation.

Finally, the remaining question is the location of the carboxylic group responsible for this spectral feature. The previous time-resolved FTIR study observed a positive carboxylic C=O stretch at 1716 $cm^{-1}$ in the $ASR_M$ minus

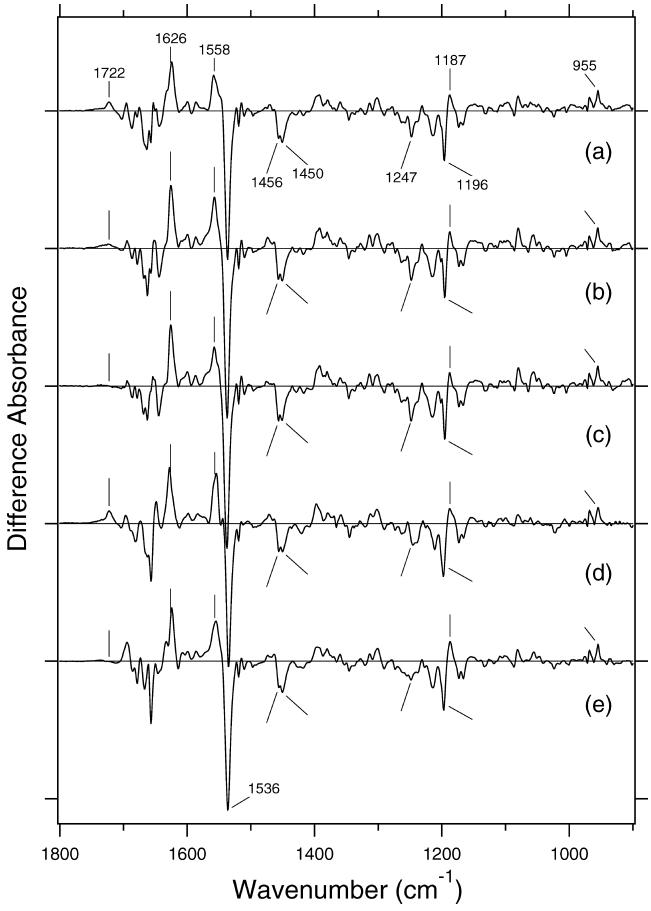


FIGURE 5: The $ASR_L$ minus ASR infrared spectra of the wild type at pH 5 (a), pH 7 (b), and pH 9 (c), D217N at pH 5 (d) and E36Q at pH 5 (e) in the 1800−900 $cm^{-1}$ region. The spectra are measured at 170 K upon hydration with $H_2O$. One division of the *y*-axis corresponds to 0.009 absorbance unit.

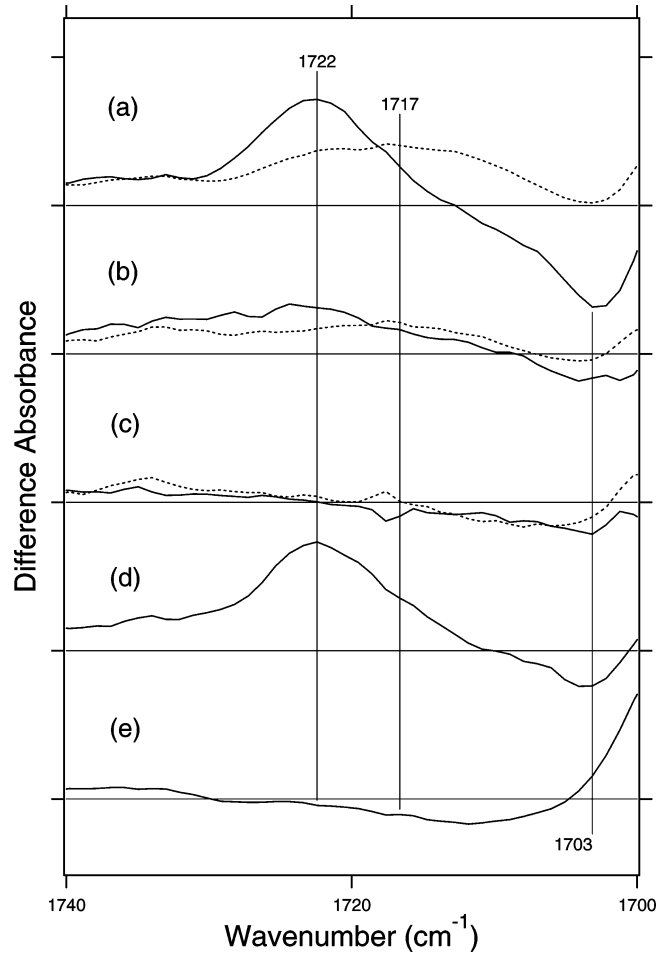


FIGURE 6: The $ASR_L$ minus ASR infrared spectra of the wild type at pH 5 (a), pH 7 (b), and pH 9 (c), D217N at pH 5 (d) and E36Q at pH 5 (e) in the 1740−1700 $cm^{-1}$ region. The sample was hydrated with $H_2O$ (solid lines) or $D_2O$ (dotted lines). One division of the *y*-axis corresponds to 0.0008 absorbance unit.

ASR spectra, and assigned the band to Asp217 located at the cytoplasmic region, because the band disappeared for D217N, but not for E36Q (*21*). Interestingly, the 1716 $cm^{-1}$ band in $ASR_M$ was also pH-dependent, whose p$K_a$ was between 6 and 7, but the pH dependence was opposite to the present case. Namely, the positive band at 1716 $cm^{-1}$ was observed at alkaline pH, but not at acidic pH, and the authors interpreted that Asp217 is protonated at acidic pH in the unphotolyzed state (*21*). They did not observe frequency change of Asp217 at acidic pH, suggesting no structural changes of Asp217 at acidic conditions. Thus, there has been no information about the C═O stretching frequency of Asp217 at acidic pH, and Asp217 is a possible candidate for the bands at 1722 (+)/1703 (−) $cm^{-1}$ in the $ASR_L$ minus ASR spectra. Here we also measured the spectra of the E36Q mutant, as Glu36 is located near Asp217 (Figure 1).

Figures 6d and 6e show the carboxylic C═O stretching region in the $ASR_L$ minus ASR spectra of D217N and E36Q, respectively. Similar difference spectra in other frequency regions ensure the normal formation of $ASR_L$ for these mutants (Figure 5). The bands at 1722 (+)/1703 (−) $cm^{-1}$ were reproduced in Figure 6d, indicating that they do not originate from Asp217. On the other hand, the bands at 1722 (+)/1703 (−) $cm^{-1}$ completely disappeared for E36Q (Figure 6e). Thus, we assigned the bands to Glu36. It is generally accepted that the C═O stretching vibrations appear at lower frequency for Glu than for Asp, but the frequency of Glu36 at 1703 $cm^{-1}$ in ASR is particularly unusual. The frequency is very low, indicating that Glu36 forms a strong hydrogen bond in the unphotolyzed state, which is weakened by structural changes upon formation of $ASR_L$ as shown by the upshift to 1722 $cm^{-1}$.

*Comparison of the Difference Infrared Spectra of the L Intermediate in Water O−D Stretching Frequency (2750−2500 $cm^{-1}$) Region.* The $ASR_L$ minus ASR spectra clearly show hydrogen-bonding alteration of Glu36. Since there is a water cluster in the cytoplasmic region near Glu36 (Figure 1), detecting water signals in the $ASR_L$ minus ASR spectrum is important. It was not easy, because $ASR_L$ decays to the 13-cis form, not to the original all-*trans* form, and the sample was dark-adapted again before the next measurement. Nevertheless, we successfully measured the spectra in the frequency region of water O−D stretching vibrations in $D_2O$. Figures 7a, 7b, and 7c show the $ASR_L$ minus ASR spectra of the wild type at pH 5, 7, and 9, respectively. The spectra show a negative peak at 2693 $cm^{-1}$ and a positive peak at 2582 $cm^{-1}$ at all pH. Since the peaks are downshifted upon hydration with $D_2{}^{18}O$, they originate from O−D stretching vibrations of water. The negative peaks at 2642 and 2628 $cm^{-1}$ in Figure 7b similarly show the isotope shift of water, indicating that they originate from water O−D stretches. Interestingly, a single peak only exists at 2642 and 2628 $cm^{-1}$

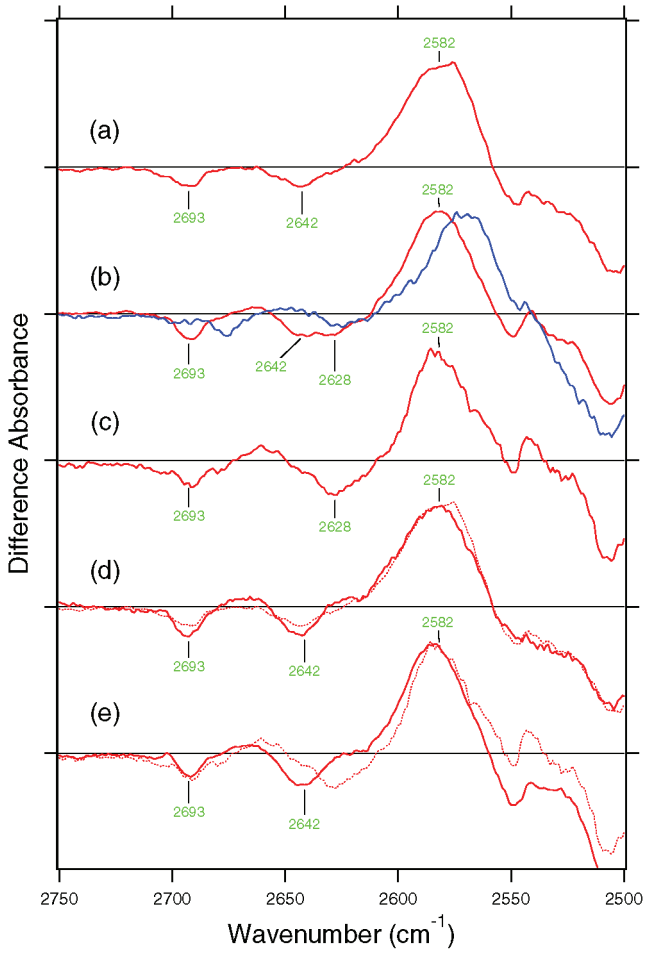


FIGURE 7: The $ASR_L$ minus ASR infrared spectra of the wild type at pH 5 (a), pH 7 (b), and pH 9 (c), E36Q at pH 5 (d) and pH 9 (e) in the 2750−2500 cm$^{-1}$ region. The dotted lines represent the spectra of the wild type at pH 5 (d) and pH 9 (e). The spectra are measured at 170 K upon hydration with $D_2O$ (red lines) or $D_2{}^{18}O$ (blue line). One division of the *y*-axis corresponds to 0.0009 absorbance unit.

for the spectra at pH 5 (Figure 7a) and pH 9 (Figure 7c), respectively. This observation implies that the frequency of the water O−D stretch is pH-dependent, being downshifted at higher pH. The p$K_a$ is located at about 7, which is coincident with that of Glu36 (Figure 6).

Similar p$K_a$ of the water O−D stretch at 2650−2620 cm$^{-1}$ to that of Glu36 suggests that the water molecule is located near Glu36. This is indeed the case, because the pH-dependence of the water O−D stretch is abolished in E36Q. Figure 7d shows identical spectra between the wild type (dotted line) and E36Q (solid line) at pH 5. However, the frequency shift of the negative band from 2642 cm$^{-1}$ to 2628 cm$^{-1}$ in the wild type at pH 9 was absent in E36Q (solid line in Figure 7e). This observation suggests that deprotonation of Glu36 at pH > 7 is correlated with the frequency shift of the water O−D stretch from 2642 cm$^{-1}$ to 2628 cm$^{-1}$. The straightforward interpretation is that the water directly interacts with Glu36. It should be noted that the water O−D stretch at 2650−2620 cm$^{-1}$ represents a weak hydrogen bond, and we presumably monitor the free O−D stretch of a water molecule interacting with Glu36.

## DISCUSSION

In this study, we report the $ASR_L$ minus ASR spectra measured by low-temperature FTIR spectroscopy. Although photoinduced current measurements of $ASR_L$ and $ASR_M$ reported the different direction of charge signal between C-terminally truncated and full-length ASR (*25*), the present FTIR study showed almost identical $ASR_L$ and ASR spectra for them (Figure 2). While the spectral features were essentially similar to those for BR, a unique feature was obtained for the carboxylic C=O stretching frequency region for ASR. The pH-dependent bands were observed at 1722 (+)/1703 (−) cm$^{-1}$ in the $ASR_L$ minus ASR spectra, which were assigned to Glu36. pH-dependent water O−D stretching vibrations in $D_2O$ were also observed at 2642 and 2628 cm$^{-1}$ for the unphotolyzed state of ASR at pH 5 and pH 9, respectively. These p$K_a$ were estimated to be between 6 and 7. According to the X-ray structure of ASR, Glu36 is located near the cytoplasmic surface (Figure 1), and the distances from the Schiff base nitrogen of the retinal chromophore to the side-chain oxygens of Glu36 are 19.3 and 20.2 Å (*16*). The present study clearly shows that formation of $ASR_L$ accompanies hydrogen-bonding alteration of Glu36. Since $ASR_L$ is formed at 170 K, this fact demonstrates structural alteration propagating over 20 Å at such low temperatures.

Spectral feature of the water signal in the $ASR_L$ minus ASR spectrum resembles that in the $BR_L$ minus BR spectrum at 2700−2500 cm$^{-1}$ (*37*). In particular, an intense positive broadband at 2630−2550 cm$^{-1}$ (O−H stretch at 3550−3450 cm$^{-1}$) has been regarded as a characteristic for the L state of BR (*37*). However, our recent time-resolved FTIR spectroscopy clearly showed the absence of the band for $BR_L$ at room temperature, and we concluded that such water signal is a low-temperature artifact, or a feature peculiar at low temperature (170 K) where L is stable (*38*). This may be also true for ASR. However, it should be noted that the cryotrapped L state is considerably relaxed to the original state in BR (*39, 40*), but decays to the subsequent intermediates in ASR by warming (*17*). This suggests different protein dynamics between ASR and BR, but room-temperature FTIR study of ASR is required for further understanding.

*Hydrogen-Bonding Structures in the Cytoplasmic Domain of ASR and $ASR_L$.* The present study showed that the p$K_a$ of Glu36 is between 6 and 7 in ASR, and its hydrogen bonding is significantly altered upon formation of $ASR_L$. Previous FTIR study reported the p$K_a$ of Asp217 being also between 6 and 7 in ASR (*21*). According to these observations, Glu36 and Asp217 are both protonated at low pH, while being both deprotonated at high pH. However, the latter may be unlikely, because Glu36 and Asp217 are located close to each other (Figure 1). Below we discuss a possible model for activation of ASR based on these observations and X-ray structure (*16*).

At low pH, Glu36 and Asp217 are both protonated in the unphotolyzed state. The hydrogen bond of Glu36 is remarkably strong (C=O stretch at 1703 cm$^{-1}$), whose hydrogen-bonding donor may be Gln93 or a water molecule (Figure 1). Upon $ASR_L$ formation, the hydrogen bond of Glu36 is weakened (C=O stretch at 1722 cm$^{-1}$). The absence of the bands for Asp217 in the $ASR_L$ minus ASR spectra (Figure 5) implies that no hydrogen-bonding alteration of this residue occurs. The hydrogen bond of a water molecule nearby

Glu36 is strengthened upon formation of $ASR_L$ as shown by the spectral shift from 2642 $cm^{-1}$ to 2582 $cm^{-1}$ (Figure 7a).

At high pH, Asp217 is probably deprotonated according to the previous results (*21*). $ASR_L$ formation does not change the hydrogen bond of Asp217, because there is no pH-dependent signal at around 1400 $cm^{-1}$ (Figure 5). Then, protonated state of Glu36 may be more likely, because negatively charged Asp217 and Glu36 are energetically unfavorable. However, the two negative charges at carboxylates could be stabilized by a positively charged water cluster ($H_3O^+$ or $H_7O_3^+$). The water structure in Figure 1 may resemble the proton release group of BR, where water cluster stabilizes Glu194 and Glu204. Experimental evidence of protonated water cluster was first reported by the group of Dr. Gerwert as a continuum band at 2200−1800 $cm^{-1}$ in the room-temperature $BR_M$ minus BR spectra (*41, 42*), and we recently identified that the continuum band contains a water signal (*38*). We did not observe such a continuum band in the $ASR_L$ minus ASR spectra at 170 K (data not shown), but this does not exclude the presence of a protonated water cluster, because the continuum band of BR is observed only at room temperature (*38*). Water-containing hydrogen-bonding network in the cytoplasmic domain (Figure 1) must play important roles in the activation of the transducer protein by ASR.

*Characteristic Features of Photoreaction in ASR.* By use of low-temperature UV−visible spectroscopy, we recently revealed that the stable photoproduct of the all-*trans* form is 100% 13-*cis*, and that of the 13-*cis* form is 100% all-*trans* (*17*). This was entirely unique for archaeal-type rhodopsins, because functionally important states known so far were only derived from the all-*trans* form, and the photocycle of the all-*trans* form without branching into the 13-*cis* stable states has been the common mechanism. The complete photocycling for the proton pump in BR and the complete photochromism for the chromatic sensor of ASR are highly advantageous for their functions. Although the protein structures are similar between ASR and BR (*16*), the present study suggests that the migration of protons to the cytoplasmic side is correlated with the unique photoreactions of ASR.

ASR has Asp75 as a counterion of the retinal chromophore, which corresponds to Asp85 in BR. Nevertheless, the Schiff base proton is transferred not to Asp75 (*21, 22*), but to Asp217 in the cytoplasmic region. What is the mechanism of proton transfer in the opposite direction? The present FTIR spectroscopy of the L intermediate revealed similar structural changes for the chromophores of ASR and BR, suggesting the importance of the surrounding protein moiety. It should be noted that Asp212 in BR is replaced by proline (Pro206) in ASR. Previous studies reported the important role of Asp212 during the M formation, and we proposed a hydration switch mechanism as the primary cause of proton transfer reaction in BR. In this mechanism, the bridged water molecule between the Schiff base and Asp85 forms a strong hydrogen bond transiently, which leads to the proton transfer to Asp85 (*37*). Lack of aspartate at position 206 would be significant for ASR. In this regard, we found the absence of strongly hydrogen-bonded water molecules in ASR (*18*). Since there is a positive correlation between the strongly hydrogen-bonded water molecules and the proton pumping activity, weakly hydrogen-bonded water molecules in the Schiff base region may be the key element. Interestingly, the replacement of Pro206 to Asp was not sufficient for ASR to function as a BR-like proton pump (*27*). Since the Schiff base proton is transferred to the cytoplasmic side, ASR is a very good model system to study the general mechanism of proton pumps in archaeal-type rhodopsins.

## REFERENCES


1. Lanyi, J. K. (1998) Understanding structure and function in the light-driven proton pump bacteriorhodopsin. *J. Struct. Biol. 124*, 164–178.
2. Essen, L. O. (2002) Halorhodopsin: light-driven ion pumping made simple? *Curr. Opin. Struct. Biol. 12*, 516–522.
3. Sasaki, J., and Spudich, J. L. (2000) Proton transport by sensory rhodopsins and its modulation by transducer-binding. *Biochim. Biophys. Acta 1460*, 230–239.
4. Kamo, N., Shimono, K., Iwamoto, M., and Sudo, Y. (2001) Photochemistry and photoinduced proton-transfer by *pharaonis* phoborhodopsin. *Biochemistry (Moscow) 66*, 1277–1282.
5. Bieszke, J. A., Braun, E. L., Bean, L. E., Kang, S., Natvig, D. O., and Borkovich, K. A. (1999) The nop-1 gene of *Neurospora crassa* encodes a seven transmembrane helix retinal-binding protein homologous to archaeal rhodopsins. *Proc. Natl. Acad. Sci. U.S.A. 96*, 8034–8039.
6. Sineshchekov, O. A., Jung, K. H., and Spudich, J. L. (2002) Two rhodopsins mediate phototaxis to low- and high-intensity light in *Chlamydomonas reinhardtii*. *Proc. Natl. Acad. Sci. U.S.A. 99*, 8689–8694.
7. Nagel, G., Ollig, D., Fuhrmann, M., Kateriya, S., Musti, A. M., Bamberg, E., and Hegemann, P. (2002) Channelrhodopsin-1: a light-gated proton channel in green algae. *Science 296*, 2395–2398.
8. Okamoto, O. K., and Hastings, J. W. (2003) Novel dinoflagellate clock-related genes identified through microarray analysis. *J. Phycol. 39*, 519–526.
9. Jung, K. H., and Spudich, J. L. (2004) Microbial rhodopsins: Transport and sensory proteins throughout the three domains of life, in *CRC Handbook of Organic Photochemistry and Photobiology* (Horspool, W. M., and Lenci F., Eds.) 2nd ed., Section II Photobiology, pp 124/1−124/11, CRC Press, Boca Raton, FL.
10. de la Torre, J. R., Christianson, L. M., Beja, O., Suzuki, M. T., Karl, D. M., Heidelberg, J., and DeLong, E. F. (2003) Proteorhodopsin genes are distributed among divergent marine bacterial taxa. *Proc. Natl. Acad. Sci. U.S.A. 100*, 12830–12835.
11. Beja, O., Aravind, L., Koonin, E. V., Suzuki, M. T., Hadd, A., Nguyen, L. P., Jovanovich, S. B., Gates, C. M., Feldman, R. A., Spudich, J. L., Spudich, E. N., and DeLong, E. F. (2000) Bacterial rhodopsin: evidence for a new type of phototrophy in the sea. *Science 289*, 1902–1906.
12. Giovannoni, S. J., Bibbs, L., Cho, J. C., Stapels, M. D., Desiderio, R., Vergin, K. L., Rappe, M. S., Laney, S., Wilhelm, L. J., Tripp, H. J., Mathur, E. J., and Barofsky, D. F. (2005) Proteorhodopsin in the ubiquitous marine bacterium SAR11. *Nature 438*, 82–85.
13. Jung, K. H., Trivedi, V. D., and Spudich, J. L. (2003) Demonstration of a sensory rhodopsin in eubacteria. *Mol. Microbiol. 47*, 1513–1522.
14. Sineshchekov, O. A., Trivedi, V. D., Sasaki, J., and Spudich, J. L. (2005) Photochromicity of *Anabaena* Sensory Rhodopsin, an Atypical Microbial Receptor with a *cis*-Retinal Light-adapted Form. *J. Biol. Chem. 280*, 14663–14668.
15. Vogeley, L., Trivedi, V. D., Sineshchekov, O. A., Spudich, E. N., Spudich, J. L., and Luecke, H. (2007) Crystal structure of the *Anabaena* sensory rhodopsin transducer. *J. Mol. Biol. 367*, 741–751.
16. Vogeley, L., Sineshchekov, O. A., Trivedi, V. D., Sasaki, J., Spudich, J. L., and Luecke, H. (2004) Anabaena sensory rhodopsin: a photochromic color sensor at 2.0 Å. *Science 306*, 1390–1393.
17. Kawanabe, A., Furutani, Y., Jung, K. H., and Kandori, H. (2007) Photochromism of *Anabaena* sensory rhodopsin. *J. Am. Chem. Soc. 129*, 8644–8649.
18. Furutani, Y., Kawanabe, A., Jung, K. H., and Kandori, H. (2005) FTIR spectroscopy of the all-*trans* form of *Anabaena* sensory rhodopsin at 77K: hydrogen bond of a water between the Schiff base and Asp75. *Biochemistry 44*, 12287–12296.

19. Sineshchekov, O. A., and Spudich, J. L. (2004) Light-induced intramolecular charge movements in microbial rhodopsins in intact *E. coli* cells. *Photochem. Photobiol. Sci. 3*, 548–554.
20. Furutani, Y., Shibata, M., and Kandori, H. (2005) Strong hydrogen-bonded water molecules in the Schiff base region of rhodopsins. *Photochem. Photobiol. Sci. 4*, 661–666.
21. Shi, L., Yoon, S. R., Bezerra, A. G., Jr., Jung, K. H., and Brown, L. S. (2006) Cytoplasmic shuttling of protons in *Anabaena* sensory rhodopsin: Implications for signaling mechanism. *J. Mol. Biol. 358*, 686–700.
22. Bergo, V. B., Ntefidou, M., Trivedi, V. D., Amsden, J. J., Kralj, J. M., Rothschild, K. J., and Spudich, J. L. (2006) Conformational changes in the photocycle of *Anabaena* sensory rhodopsin: Absence of the Schiff base counterion protonation signal. *J. Biol. Chem. 281*, 15208–15214.
23. Kandori, H. (2004) Hydration switch model for the proton transfer in the Schiff base region of bacteriorhodopsin. *Biochim. Biophys. Acta 1658*, 72–79.
24. Shibata, M., Yoshitsugu, M., Mizuide, N., Ihara, K., and Kandori, H. (2007) Halide binding by the D212N mutant of bacteriorhodopsin affects hydrogen bonding of water in the active site. *Biochemistry 46*, 7525–7535.
25. Sineshchekov, O. A., Spudich, E. N., Trivedi, V. D., and Spudich, J. L. (2006) Role of the cytoplasmic domain in *Anabaena* sensory rhodopsin photocycling: Vectoriality of schiff base deprotonation. *Biophys. J. 91*, 4519–4527.
26. Kawanabe, A., Furutani, Y., Jung, K. H., and Kandori, H. (2006) FTIR study of the photoisomerization processes in the 13-*cis* and all-*trans* forms of *Anabaena* sensory rhodopsin at 77 K. *Biochemistry 45*, 4362–4370.
27. Choi, A. R., Kim, S. Y., Yoon, S. R., Bae, K., and Jung, K. H. (2007) Substitution of Pro206 and Ser86 residues in the retinal binding pocket of *Anabaena* sensory rhodopsin is not sufficient for proton pumping function. *J. Microbiol. Biotechnol. 17*, 138–145.
28. Jung, K. H., and Spudich, J. L. (1996) Protonatable residues at the cytoplasmic end of transmembrane helix-2 in the signal transducer HtrI control photochemistry and function of sensory rhodopsin I. *Proc. Natl. Acad. Sci. U.S.A. 93*, 6557–6561.
29. Jung, K. H., Spudich, E. N., Trivedi, V. D., and Spudich, J. L. (2001) An archaeal photosignal-transducing module mediates phototaxis in *Escherichia coli*. *J. Bacteriol. 183*, 6365–6371.
30. Kandori, H., Shimono, K., Sudo, Y., Iwamoto, M., Shichida, Y., and Kamo, N. (2001) Structural changes of *pharaonis* phoborhodopsin upon photoisomerization of the retinal chromophore: infrared spectral comparison with bacteriorhodopsin. *Biochemistry 40*, 9238–9246.
31. Aton, B., Doukas, A. G., Callender, R. H., Becher, B., and Ebrey, T. G. (1977) Resonance Raman studies of the purple membrane. *Biochemistry 16*, 2995–2999.
32. Smith, S. O., Braiman, M. S., Myers, A. B., Pardoen, J. A., Courtin, J. M. L., Winkel, C., Lugtenburg, J., and Mathies, R. A. (1987) Vibrational analysis of the all-trans-retinal chromophore in light-adapted bacteriorhodopsin. *J. Am. Chem. Soc. 109*, 3108–3125.
33. Gerwert, K., and Siebert, F. (1986) Evidence for light-induced 13-cis, 14-s-cis isomerization in bacteriorhodopsin obtained by CFIR difference spectroscopy using isotopicaily labelled retinals. *EMBO J. 5*, 805–811.
34. Mathies, R. A., Smith, S. O., and Pollard, W. T. (1987) in *Biological applications of Raman spectroscopy: Resonance Raman spectra of polyenes and aromatics* (Spiro, T. G., Ed.) pp 59−108, John Wiley and Sons, New York.
35. Maeda, A., Sasaki, J., Pfefferle, J. M., Shichida, Y., and Yoshizawa, T. (1991) Fourier transform infrared spectral studies on the Schiff base mode of all-*trans* bacteriorhodopsin and its photointermediates, K and L. *Photochem. Photobiol. 54*, 911–921.
36. Braiman, M. S., Mogi, T., Marti, T., Stern, L. J., Khorana, H. G., and Rothschild, K. J. (1988) Vibrational spectroscopy of bacteriorhodopsin mutants: Light-driven proton transport involves protonation changes of aspartic acid residues 85, 96, and 212. *Biochemistry 27*, 8516–8520.
37. Tanimoto, T., Furutani, Y., and Kandori, H. (2003) Structural changes of water in the Schiff base region of bacteriorhodopsin: Proposal of a hydrogen switch model. *Biochemistry 42*, 2300–2306.
38. Lorenz-Fonfria, V. A., Furutani, Y., and Kandori, H. (2008) Active internal waters in the bacteriorhodopsin photocycle. A comparative study of the L and M intermediates at room and cryogenic temperatures by infrared spectroscopy. *Biochemistry 47*, 4071–4081.
39. Litvin, F. F., Balashov, S. P., and Sineshchekov, V. A. (1975) The investigation of the primary photochemical conversions of bacteriorhodopsin in purple membranes and cells of *Halobacterium halobium* by the low temperature spectrophotometry method. *Bioorg. Khim. 1*, 1767–1777.
40. Dioumaev, A. K., and Lanyi, J. K. (2007) Bacteriorhodopsin photocycle at cryogenic temperatures reveals distributed barriers of conformational substates. *Proc. Natl. Acad. Sci. U.S.A. 104*, 9621–9626.
41. Rammelsberg, R., Huhn, G., Lubben, M., and Gerwert, K. (1998) Bacteriorhodopsin's intramolecular proton-release pathway consists of a hydrogen-bonded network. *Biochemistry 37*, 5001–5009.
42. Garczarek, F., Brown, L. S., Lanyi, J. K., and Gerwert, K. (2004) Proton binding within a membrane protein by a protonated water cluster. *Proc. Natl. Acad. Sci. U.S.A. 102*, 3633–3638.

BI800941A